JACS
JOURNAL OF THE AMERICAN CHEMICAL SOCIETY

Article

pubs.acs.org/JACS

Association Dynamics and Linear and Nonlinear Optical Properties of an *N*-Acetylaladanamide Probe in a POPC Membrane

N. Arul Murugan,[†] Rossen Apostolov,[‡,∥] Zilvinas Rinkevicius,[†] Jacob Kongsted,[§] Erik Lindahl,[∥,⊥] and Hans Ågren*[,†]

[†]Division of Theoretical Chemistry and Biology, School of Biotechnology, Royal Institute of Technology, SE-10691 Stockholm, Sweden

[‡]PDC Center for High Performance Computing, School of Computer Science and Communication, Royal Institute of Technology, SE-10691 Stockholm, Sweden

[§]Department of Physics, Chemistry and Pharmacy, University of Southern Denmark, Campusvej 55, DK-5230 Odense M, Denmark

[∥]Department of Biochemistry and Biophysics, Science for Life Laboratory, Stockholm University, SE-171 21 Solna, Sweden

[⊥]Theoretical and Computational Biophysics, Department of Theoretical Physics, Royal Institute of Technology, Stockholm, Sweden

Supporting Information

ABSTRACT: Along with the growing evidence that relates membrane abnormalities to various diseases, biological membranes have been acknowledged as targets for therapy. Any such abnormality in the membrane structure alters the membrane potential which in principle can be captured by measuring properties of specific optical probes. There exists by now many molecular probes with absorption and fluorescence properties that are sensitive to local membrane structure and to the membrane potential. To suggest new high-performance optical probes for membrane-potential imaging it is important to understand in detail the membrane-induced structural changes in the probe, the membrane association dynamics of the probe, and its membrane-specific optical properties. To contribute to this effort, we here study an optical probe, *N*-acetylaladanamide (NAAA), in the presence of a POPC lipid bilayer using a multiscale integrated approach to assess the probe structure, dynamics, and optical properties in its membrane-bound status and in water solvent. We find that the probe eventually assimilates into the membrane with a specific orientation where the hydrophobic part of the probe is buried inside the lipid bilayer, while the hydrophilic part is exposed to the water solvent. The computed absorption maximum is red-shifted when compared to the gas phase. The computations of the two-photon absorption and second harmonic generation cross sections of the NAAA probe in its membrane-bound state which is of its first kind in the literature suggest that this probe can be used for imaging the membrane potential using nonlinear optical microscopy.

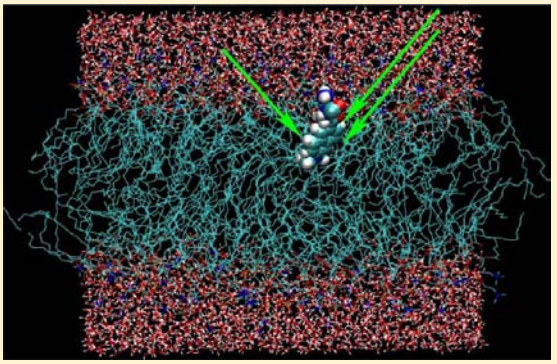

1. INTRODUCTION

Cell membranes are natural targets for modern molecular probing technology, as they play an active role in transferring molecules into or out of the cells.[1] This transfer is commonly assumed to be effectuated by an electrostatic potential that builds up over the membrane. There are a number of ambiphilic dyes which spontaneously penetrate into a lipid membrane and change their properties as a result of this potential and a varying local environment.[2] Such dyes are widely used to visualize variations in the cell membranes. Within the channels there is alignment of dipole moments of the lipid head groups and water, leading to a dipolar potential which can modify the total electrostatic potential across the membrane.[3] In light of these findings a natural question arises concerning the underlying causes of the observed salient changes of the properties of a probe when immersed in a cell channel and how that response can lead to information on structure and electrostatic potential across the membrane or microfields within the membrane. This in turn refers to the nature of the perturbation of the probes: i.e., if the property change is mostly due to direct perturbation of the electronic structure of the probe or shifting charge (electrochromic mechanisms) by the interaction with the environment or is indirect where the environment either perturbs the alignment of the probe (solvatochromic mechanisms), n.b. their dipoles, or leads to intrinsic structural changes in the probe that in turn give rise to spectral shifts.[4] The contributions to linear and nonlinear optical properties of the molecular probes due to the changes in the intrinsic structure have been often reported to be dramatic.[4] Even for peptides, the effect of intrinsic structure on the nonlinear optical properties has been observed, and the

Received: July 17, 2013
Published: August 16, 2013

   dx.doi.org/10.1021/ja407326n | *J. Am. Chem. Soc.* 2013, 135, 13590−13597

peptides with β strand structure have larger first hyperpolarizability than the α helix.[5] Earlier studies on solvents and other confined environments, like protein pockets or DNA grooves, have clearly indicated the importance of the solvatochromic mechanism. Other factors like solvent polarity, pH, and ionic strength have also been proposed. Furthermore, viscosity changes and solvent-dependent aggregation effects have also been put forward as causes for salient changes in the response of the membrane probes. Although the voltage sensing has been suggested to depend on combinations of several such mechanisms it seems that the orientation factor has received the greatest attention, albeit with some controversy. Apart from mechanisms of spectral response the issue on how to translate that response to information on probe location is pertinent, i.e., possible location in the headgroup region, away from the water-accessible region, or central in the membranes. These positions may alter considerably by incorporation of a drug molecule. The most popular technique to probe these issues is fluorescence spectroscopy, where fluorescence intensity, lifetime, and anisotropy provide measurable quantities. More recent studies have also introduced nonlinear optical spectroscopies like two-photon excitation fluorescence (TPEF)[6,7] and second harmonic generation (SHG),[8] and such techniques have now received considerable attention, in the first case much owing to the penetrating and focusing nature of the process and in the latter case much owing to its strong directional character and dependence on orientation of the microfields in the membrane.

The research on voltage-gated membrane channels and membrane probes poses considerable interest but also challenges for theory and modeling. Most modeling studies have concerned structure and dynamics through classical atomistic or coarse-graining models, where the former, n.b. molecular dynamics (MD), by virtue of technical advances now are capable to treat models with more than one million atoms.[9] Spectroscopically, most work is done by limited models cut out from MD snapshots, either by time-dependent density functional theory (TD-DFT) or ab inito methodologies, in the latter case severely limiting the size of the systems. A theme of the present work is that salient problems with respect to membrane channel probing can advantageously be addressed by recent advances of quantum-classical modeling including all aspects of structure, dynamics, properties, and spectroscopic response of biomolecules in complex environments. Such modeling also opens new avenues for designing molecular probes for specific applications. In particular, so-called quantum mechanics/molecular mechanics (QM/MM) methods are now capable to analyze molecular probes covering spectroscopies over a wide range of wavelengths and for a variety of types of environments.[10] Applications have so far though mostly concerned probes in solvents and confined environments like DNA and proteins.[11,12] Such calculations are often executed through the so-called integrated approach[10,12,13] where the conformations of the full system are sampled dynamically followed by calculations of the spectral property of interest over trajectories of uncorrelated configurations from the sampling. Such a technology is now capable of addressing a number of problems of the intrinsic action of the probes. To address these challenges and reach some understanding of the information given by membrane probes, we apply the aforementioned QM/MM modeling to a selected membrane−probe system, namely, the 1-palmitoyl-2-oleoyl-sn-glycero-3-phosphocholine (POPC) lipid bilayer−*N*-acetylaladanamide (NAAA) (see Figure 1). As

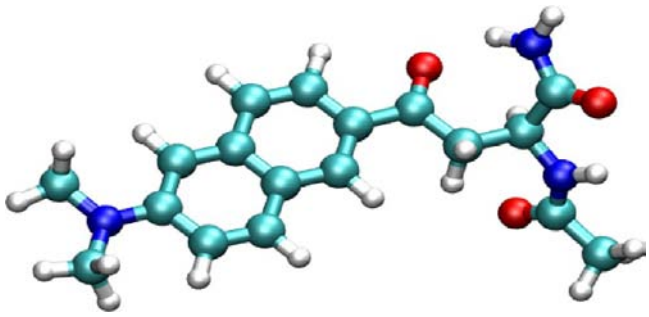

Figure 1. Molecular structure of the NAAA probe.

the first step we employ in the integrated approach extensive molecular dynamics sampling of possible structures and apply QM/MM with the molecular probe as the QM part and the membrane atoms and water in the MM part. Full interaction (thus all types of molecular interaction contributions) within and between the two parts is accounted for in forming the spectrum of the probe.

The reason for choosing the molecular dynamics approach for structure modeling is because the membrane association process of probes is a long time scale process. As the membrane is embedded in water solvent, we start with an initial configuration where the probe is immersed in the water solvent. The chosen probe has molecular geometry similar to prodan[14−19] and laurdan[20,21] which have been extensively used to probe membrane structure. This has motivated us to study it as a demonstration case for membrane probing applications even though the available experimental data for this probe mostly are connected to dielectric probing of protein microenvironments.[22,23] We have aimed to study whether it has a tendency to bind to the membrane and whether it has any membrane-specific optical property. Finally, we have also addressed its potency to be used as two photon absorption (TPA) and SHG probes[24] due to the promising recent reports on prodan derivatives as TPA probes for membranes.[21,25−27]

2. COMPUTATIONAL DETAILS

Below we describe in some detail the integrated approach which is used to simulate structure, dynamics, and linear and nonlinear optical properties of the probe within the membrane. All the QM/MM calculations rely on the use of DFT for the QM core and TD-DFT for the excited state properties.

2.1. Molecular Dynamics Simulations. As a starting structure for the model we used a pre-equilibrated solvated (3572 water molecules) lipid bilayer of 128 POPC chains. A NAAA molecule was placed in the bulk water at 0.5 nm from the bilayer surface with the long axis of the molecule parallel to the membrane surface. The NAAA topology was generated using the GAFF force field[28] and partial charges calculated using the CHELPG procedure[29] as implemented in the Gaussian09 software.[30] The lipid bilayer was modeled using the Berger lipid parameter set[31] and SPC/E parameters for water.[32] Bonds were restrained according to the LINCS algorithm to allow for timesteps of 2 fs. Long-range electrostatic interactions were computed with the PME method with 1.2 nm cutoff and updates to the neighbor list done every 10 steps. The water and the probe molecule were coupled separately from the lipids to a heat bath of 303 K using the velocity rescale thermostat developed by Bussi.[33] Atmospheric pressure of 1 bar was controlled by a Parrinello−Rahman barostat[34] with a time constant of 5 ps and compressibility 4.5×10^{-5}. The system was equilibrated for 1 ns with position restraints on the NAAA heavy atoms to allow for relaxation of the solvating bulk water. The restraints were released for a production run of 50 ns. Trajectory

dx.doi.org/10.1021/ja407326n | J. Am. Chem. Soc. 2013, 135, 13590−13597

snapshots were taken every 10 ps. Simulations, modeling, and analysis were carried out with the Gromacs v4.5.5 simulation package.[35]

2.2. Hybrid TD-DFT/MM Calculations. The calculations to compute linear and nonlinear optical properties were restricted to 100 configurations from the total stored 5000 configurations since this set of calculations is computationally demanding. Moreover, an averaging over 50−100 uncorrelated configurations has been shown to give converged results for properties from earlier studies on other systems.[11,12] The property calculations were done using a hybrid TD-DFT/MM approach employing the polarizable embedding scheme[36] to describe the two subsystem interactions, namely, the probe and the membrane. The NAAA probe is described using density functional theory, while the membrane and water are described using molecular mechanics force fields. Since the membrane system is homogeneous only along the XY directions, instead of a routinely used spherical cutoff we employed a cylindrical cutoff for the membrane while we employed a spherical cutoff for solvents. We refer to Figures S1 and S2 of the Supporting Information which represent typical snapshots used in the TD-DFT/MM calculations. They correspond, respectively, to the two cases of the probe immersed in water and the probe associated to the membrane. The water solvent and membranes within 15 Å cutoff from the probe center of mass are included in the MM region. We have computed the one- and two-photon properties of this probe using the TD-DFT/MM response approach. In particular, one-photon absorption properties are computed from linear response calculations, while the two-photon absorption properties are computed from the first residue of the quadratic response function. The force fields used in the TD-DFT/MM calculations are the same as the ones used in the preceding MD simulation. All TD-DFT calculations are based on the use of the CAM-B3LYP exchange-correlation functional and the Turbomole-TZVP basis set.

3. RESULTS AND DISCUSSION

3.1. Membrane Association Dynamics of the NAAA Probe. A molecule to be used as a probe to target a specific biostructure within the human body should fulfill a few criteria such as: (i) exhibiting binding specificity toward the target biostructure; (ii) exhibiting characteristic optical properties in the target−biostructure bound state; and (iii) revealing information about the microenvironment of the biostructure without introducing any dramatic changes in it. In other words, the probe should be small and sensitive and should not introduce any appreciable structural changes in the biostructure. The most well-celebrated examples refer to the thioflavin-T (THT) like optical probes that are used to stain fibrils.[37] In the fibril-bound state THT shows a red-shift in its absorption spectrum, and it also exhibits a manifold increase in the fluorescence intensity. The usually known protocol to study the binding affinity and mode of binding of the probe is to use molecular docking. However, this is suitable for biostructures with well-defined binding cavities/sites like proteins, fibrils, or DNA, while such procedures cannot be employed for a membrane. The only way to study the binding mode of the probe and its association dynamics to membranes is by performing a long time scale molecular dynamics simulation with a total time scale larger than that needed for the membrane association process. Because of this, we have carried out molecular dynamics for 50 ns starting from an initial configuration where the NAAA probe is placed in the water solvent on the surface of the lipid bilayer (see Figure 2a). Interestingly, by 10 ns the NAAA probe starts to enter into the membrane (see Figure 2b) and remains there until the completion of the entire simulation (see Figure 2c). The average density as a function of z-axis which is typical for a membrane bilayer is shown in Figure S3 (Supporting Information). To follow the dynamics of the NAAA probe we have computed the time evolution of the center of mass components of the probe; the results are shown in Figure S4 (of the Supporting Information). Large variations are seen in all three (X, Y, and Z) components of the center of mass until after 10 ns simulation when some components tend to stabilize with time. This clearly means that until 10 ns the probe has large amplitude motion which tends to become localized due to the membrane association process. Even though a converged behavior is seen in the X component, there is some variation in the other two components which suggests that even within the membrane the molecule, still being fully localized, can have sliding motion without disrupting the membrane structure. In other words, within the membrane the molecular motion is restricted along some molecular axis, while in other directions it tends to remain the same as in water solution.

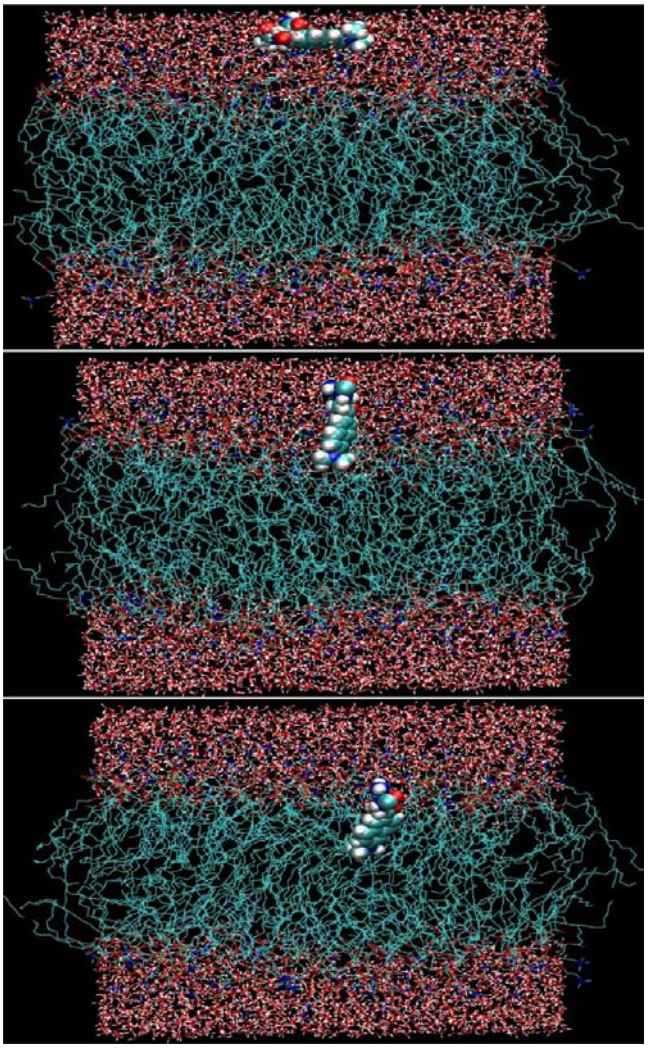

Figure 2. Three different representative snapshots of the membrane association process of the probe.

The three most important stages of the membrane association process of the probe are shown in Figure 2a−c. We aim to understand the driving force for such an association process by computing the time evolution of the van der Waals and electrostatic interactions (which adds to the total interaction energy of the system); the results are shown in Figure 3. In particular, the contributions have been separately calculated for the probe−solvent and probe−membrane

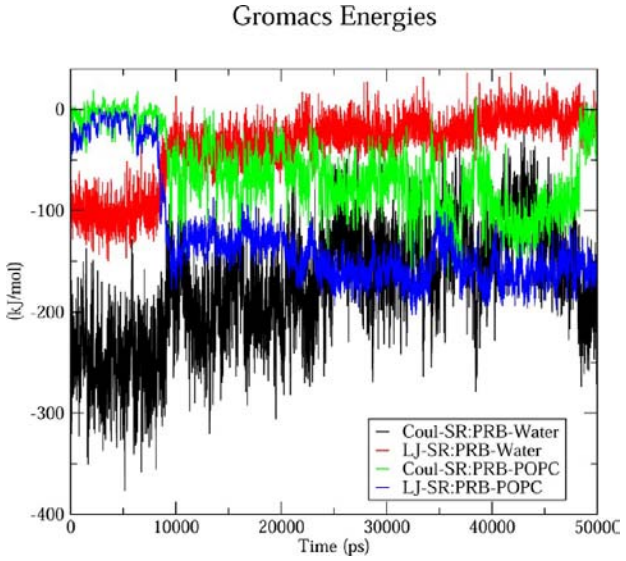

Figure 3. van der Waals and electrostatic contributions to probe−water and probe−membrane interactions as a function of time. Below 10 ns, the probe−water interaction dominates, while after this the probe−membrane interaction dominates.

systems. It can clearly be noticed from the time evolution of the interaction energies that there are remarkable changes occurring around 10 ns which we thus attribute to the membrane association of the probe. Until 10 ns, the probe−membrane contributions to the total interaction energy are negligible, and it mostly receives contributions by the probe−water interactions. It is also interesting to notice that, within the probe−water interaction, the electrostatic contribution is dominant when compared to the van der Waals term which suggests that below 10 ns the probe−membrane−water system has large contributions coming from the hydrophilic interaction between the probe and water solvent. However, after 10 ns, the contributions from the probe−membrane interactions become significant. Interestingly, the probe−membrane interaction has dominant contributions from the van der Waals rather than from the electrostatic part which is just opposite to the case of the probe−water subsystem below 10 ns. This clearly conveys a picture that the probe−membrane interactions are mostly hydrophobic in nature, while the probe−solvent interactions have large hydrophilic character. A similar observation where the probe interaction with fibrils was driven by hydrophobic interaction was reported by us recently in the case of oligothiophene conjugate nitroxide spin label−amyloid fibrils.[38] It is also important to notice that even after 10 ns the probe−water electrostatic contributions are still significant which suggests that the polar group of the membrane might be surrounded by water, contributing to a significant interaction energy. However, the number of solvent molecules surrounded by the NAAA probe should clearly be reduced when the probe is associated to the membrane. For this reason we have computed the radial distribution function (rdf) based on all atoms of NAAA and center of mass of the solvent which is shown in Figure S5 of the Supporting Information. The rdf exhibits three different shoulders which we attribute to different solvation shells. The first solvation shell corresponds to a distance less than 2.5 Å, while the distance criteria for the second and third solvation shells are 4.6 and 7 Å, respectively. We have computed the time evolution of the number of solvent molecules in different solvation shells, and the results are shown for the second and third solvation shells in Figure S6 of the Supporting Information. As it can be seen, beyond 10 ns there is a dramatic change in the average number of solvent molecules in the second and third solvation shells. The changes in the first solvation shell were less dramatic, and this explains why the probe−water electrostatic interaction tends to remain significant even after the membrane association process.

The number of solvent molecules in the second solvation shell before the membrane association process of the probe is approximately 80 which reduces to 25−40 after this process. This is in fact similar to the observation we have made in the case of the THT probe which showed a 33−50% decrease in the solvent molecules in the solvation shell when it is bound to a fibril.[12] The mode of binding of the probe has been a topic of discussion in the case of prodan which is shown to give evidence for both cases; in the first case the dimethylamino and anthracene groups are buried inside, and in the other case the carbonyl group and anthracene groups enter into the membrane.[18] Here, in the present case, the dimethylamino group and the anthracene groups are buried inside the membrane, something that seems reasonable considering the bulky groups attached to the carbonyl group.

3.2. One- and Two-Photon Optical Properties of the Probe. Originally, the NAAA probe has been synthesized for probing the dielectric nature of different cavities (such as fully buried, partly exposed, and fully exposed) within a protein.[23] Its fluorescence spectra show a strong dependence on the dielectric nature of the microenvironment. The emission maximum has been observed in the range 468−525 nm depending upon the location of the probe within the protein. However, the absorption maximum has not shown any strong dependence upon the dielectric nature of the binding sites. The absorption maximum for the NAAA probe in the presence of protein binding cavities has been reported to be around 360 nm.[22,23] Due to the large number of reports of the structurally similar prodan-like molecules for membrane probing,[14,15,20] we aimed to study its membrane-bound state-specific optical properties, in particular its absorption spectra in the presence of the POPC lipid bilayer and when it is in water solvent prior to its membrane association. In particular, we have studied whether the indirect media effects contribute to the absorption spectra of the probe. To accomplish this also the excitation energies were computed for the probe geometry alone without including the environment (denoted as set MM-0). Along with this the excitation energy calculations were carried out with the environment included explicitly (set MM-1). The average values from the MM-0 and MM-1 sets are given in Table 1 which also includes the excitation energies computed for the optimized gas-phase geometry of the probe. In particular, the

Table 1. Average Excitation Energy and Shift When Compared to in Vacuum[a]

	system		
excitation	gas	MM-0	MM-1
1	321 (0.45)	327 (0.18)	332 (0.26)
2	304 (0.05)	311 (0.02)	312 (0.04)
3	294 (0.00)	304 (0.06)	297 (0.00)
4	254 (0.46)	254 (0.71)	260 (0.60)

[a]Results are given in nanometers, and the oscillator strengths are provided in parentheses.

dx.doi.org/10.1021/ja407326n | J. Am. Chem. Soc. 2013, 135, 13590−13597

excitation energy and the corresponding oscillator strength of the four lowest transition energies are given. The absorption spectra computed by convoluting the bands associated with these excitations are shown in Figure 4. The standard

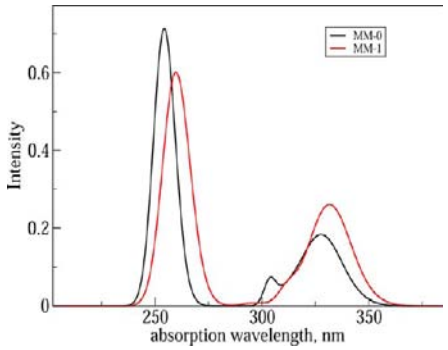

Figure 4. Absorption spectra (obtained by convoluting the four lowest transitions) computed using the MM-0 and MM-1 models.

deviations in excitation energies have been used to calculate the full-width half-maximum of the line shape functions. Among the four excitations, the first and the fourth have relatively strong intensity. When compared to the gas-phase value for the absorption maximum for the lowest energy excitation, the MM-1 values are red-shifted approximately by 11 nm. The average value from MM-0 appears between the gas phase and MM-1 value suggesting that the contributions from indirect media effects are significant, leading to a red shift in the excitation energy of the first excitation band.

Due to its structural similarity with NAAA, it is relevant to compare the above given results with those of the solvent-dependent absorption spectra of prodan.[17] When going from a cyclohexane-like environment to water, a red-shift which amounts to 15 nm has been observed in the case of prodan.[17] We report also a red shift for NAAA (by 11 nm) for going from vacuum to the membrane-bilayer-like heterogeneous environment. We have analyzed the nature of the lowest energy electronic transition involving the HOMO and LUMO levels. In Figure S7 of the Supporting Information the HOMO and LUMO orbitals involved in this excitation are shown. The former is of π type with an electron density localized on the naphthalene aromatic moiety and on the dimethylamino group. The LUMO orbital has π^* character with electron density localized on the aromatic moiety as well as on the carbonyl group. The excitation appears to have $\pi \rightarrow \pi^*$ character with some intramolecular charge-transfer character from the dimethylamino group to the amide group. We refer to the electron density localized on the dimethylamino group in the HOMO (as shown in Figure S7b of the Supporting Information), and in the case of LUMO it is localized on the amide group (as shown in Figure S7a of the Supporting Information). A red-shift in the absorption spectra is usually attributed to an increased stabilization of the excited state relative to the ground state suggesting that the excited state molecular dipole moment is larger than the ground state dipole moment.[4] This is in fact the observed general behavior in all positive solvatochromic molecules.[4] Accordingly, the computed difference in dipole moments of the excited and ground state is rather significant (6.4 D) and comparable to the change in dipole moment (7 D) reported in the case of prodan which in fact is structurally similar to NAAA.[25]

Concerning bioimaging of living cells, the wavelength of relevance is either the near-IR or IR regions of the spectrum. However, as we see from the above discussion NAAA absorbs by near-UV light which might cause damage to cells. Here two-photon excitation spectroscopy can be used to alleviate the problem.[6,7,24] In this technique, the molecule is excited using two photons of the same frequency, making it possible to apply radiation in the near-IR or IR regions. The property of relevance is the two-photon absorption cross sections which must be sufficiently large to allow the usage of microscopy (TPM).[39] Interestingly, prodan-like molecular probes have already been experimentally used in studies of membrane structure using TPM. In particular, laurdan and C-laurdan, which are prodan derivatives, have been used to visualize lipid rafts, DPPC, and DOPC membranes.[21,27] The peak of two-photon absorptivity has been reported in the 50−60 and 150−320 GM range for laurdan and C-laurdan, respectively.[21,27] Due to these proposals of prodan derivatives as suitable TPA probes, we have studied two-photon absorption properties of NAAA for application as a membrane probe. The TPA values (in GM

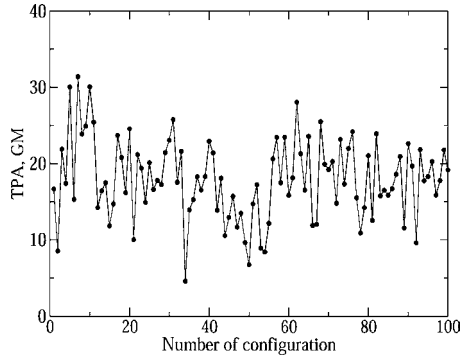

Figure 5. Time evolution of TPA of the probe. The snapshots corresponding to 20 and less than that correspond to the case where the probe is embedded within water, and the other remaining configurations correspond to the case where the probe is bound to the membrane.

unit) for 100 configurations, shown in Figure 5, are computed using the following expression

$$\delta_{GM} = \frac{(2\pi)^3 \alpha a_0^5 \omega^2}{c\pi\Gamma}\delta_{au} \quad (1)$$

Here α is the fine structure constant; a_0 is the Bohr radius; Γ is the width of the Lorentzian-shape absorption profile; ω is the energy of the photon; and c is the speed of the light. In many TPA studies, Γ is chosen to be 0.24 eV.[40,41] However, we have calculated this value using the line-shape function of the one-photon absorption spectra; the details are described in our previous paper.[42] As can be seen, the TPA values vary from 4 to 32 GM with an average corresponding to 18 GM. The maximum in two-photon absorption is 32 and 28 for the cases of probe within water and the probe within membrane, respectively. As we have discussed, the configurations up to 20 correspond to the probe embedded in water after which it goes into the membrane. When compared to laurdan and C-laurdan the computed TPA values are smaller, and some structural modification of NAAA is essential to be used as a TPA probe. For this reason, we have computed the molecular quantities

dx.doi.org/10.1021/ja407326n | J. Am. Chem. Soc. 2013, 135, 13590−13597

appearing in a two-state model (2SM) for the TPA property as shown in the following equation.

$$\delta^{2SM} = \frac{16}{15}\frac{|\mu^{01}|^2|\Delta\mu|^2}{\omega^2}(1 + 2\cos^2\theta_{\Delta\mu}^{\mu^{01}}) \quad (2)$$

Here, μ^{01} and $\Delta\mu$ refer to the transition dipole moment from the ground to the first excited state and the difference between the excited and ground state dipole moments, respectively. The $\theta_{\Delta\mu}^{\mu^{01}}$ refers to the angle between these two vectors, while the ω refers to the excitation energy. All these quantities have been computed for the optimized geometry of NAAA in isolation and are presented in Table 2. As can be seen, the large value for

Table 2. Two-State Model Analysis Parameters[a]

system	μ_{01}	$\Delta\mu$	$\theta_{\Delta\mu}^{\mu_{01}}$	ω	$\delta^{2SM} \times 10^3$
NAAA	2.17	2.53	157.24	0.142	4.31 (5.56)

[a]All numbers are reported in au. The numbers in parentheses refer to results based on response theory calculations including all possible states within the given one-electron basis set.

the transition dipole moment and difference in dipole moment and their close to parallel alignment contributes to the significant TPA value. The 2SM model predicted value for δ is 4.3×10^3, while the one calculated from response theory is 5.6×10^3, which are comparable, suggesting that the two-photon absorption process is dominated only by the ground and the first excited state. By structural tuning one can probably increase the charge transfer which might lead to the increase in $\Delta\mu$, and eventually this should increase δ. The intramolecular charge transfer has been discussed in terms of spatial overlap, Λ, computed for the two molecular orbitals involved in the particular excitation process.[41] A large spatial overlap corresponds to a localized nature of the excitation, while a small value indicates a charge transfer character.[43] Originally, Λ has been proposed as a diagnostic parameter for the usage of different functionals to explain the charge transfer excitation.[43] Since this parameter quantifies the charge transfer character of a particular excitation, we have analyzed whether this quantity shows correlation to the obtained TPA value. The results are displayed as a scatter diagram in Figure 6, where the x-value refers to spatial overlap and the TPA values are shown on the y axis. A fairly good linear relationship is seen between the spatial overlap and TPA values, suggesting that this quantity can be used as a key parameter for designing molecules with larger TPA cross sections. The black circles in this figure show the averaged TPA value for spatial overlap separated by 0.05. The straight line shows a linear fitting to the scattered data which in fact overlaps with the averaged TPA values for a given range of spatial overlap.

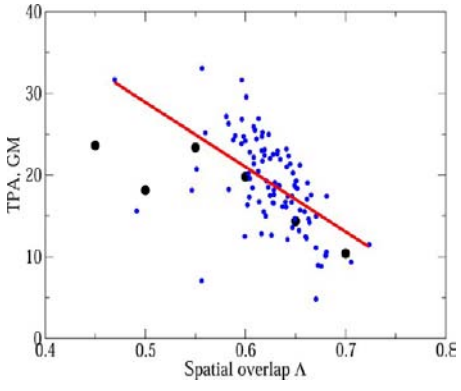

Figure 6. Scatter diagram of spatial overlap (computed for the HOMO and LUMO orbitals involved in the low-energy excitation) and TPA values which appear to have a linear relationship.

3.3. Second Harmonic Generation Properties of the Probe. Recently, simultaneous measurements of signals from two-photon excited fluorescence and second harmonic generation[7,44,45] have been put forward for high-resolution imaging of molecular probes localized in complex biostructure. In such context, the molecular probes should possess a large TPA cross section and also a large first-order hyperpolarizability. We have already shown that NAAA carries a reasonable TPA value associated with excitations to the lowest excited electronic state. Here, we have also computed the first hyperpolarizabilities for NAAA in water and in the membrane. The results as a function of number of configurations (along with the N-point averages) are shown in Figure 7. For the first hyperpolarizability the following quantity has been computed

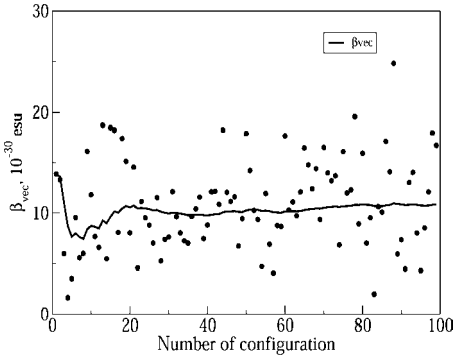

Figure 7. Time evolution of β_{vec} (in 10^{-30} esu).

$$\beta_{vec} = \frac{3}{5}\sum_{i=1}^{3}\frac{\mu_i\beta_i}{|\mu_i|} \quad (3)$$

$$\beta_i = \beta_{iii} + \frac{1}{3}\sum_{j\neq i}(\beta_{ijj} + \beta_{jij} + \beta_{jji}) \quad i, j \in (x, y, z) \quad (4)$$

Here, μ is the ground state molecular dipole moment. β_{vec} is the vector component of β projected along the direction of the dipole moment and is sampled experimentally in electric field-induced second harmonic generation experiments.[46,47] These properties are given in the molecular frame and thus are a direct measure of molecule nonlinear optical activity independent of geometrical arrangement of experimental setup.

As shown, NAAA exhibits significant β_{vec} and can so be used as a potential probe for simultaneous TPM and SHG imaging. However, as for the two-photon spectroscopy, some structural tuning would be desirable to increase further the intramolecular charge transfer. This would increase the difference in dipole moment and so the first hyperpolarizability and TPA cross section since this term appears in the numerator of the two-state models for first hyperpolarizability and TPA cross section.[39,46,47]

dx.doi.org/10.1021/ja407326n | J. Am. Chem. Soc. 2013, 135, 13590−13597

4. CONCLUSIONS

Abnormalities in membrane structures have commonly been attributed to diseases making their probing useful for diagnosis. There exists a variety of molecular probes that can associate to membranes but also disrupt their structure. Because of this circumstance there is an increasing demand for small molecular probes with membrane binding ability to be used for optical microscopy imaging techniques, where in particular those based on nonlinear response, like coherent two-photon absorption or second harmonic generation, show intriguing possibilities. Here, we have studied the potential of a well celebrated protein-dielectric probe, *N*-acetylaladanamide, as a candidate for such membrane nonlinear optical imaging. Significant TPA values and β_{vec} computed for the probe suggest that this probe indeed can be used for simultaneous TPA and SHG imaging of the membrane which is in fact a recent development in the membrane imaging technology. Our proposal is based on a combined molecular dynamics and hybrid quantum mechanics/molecular mechanics approach where the former technique is used to study the membrane association dynamics of the probe while the latter is used to compute its one- and two-photon absorption and second harmonic generation properties. To the best of our knowledge, this is the first time the integrated approach has been used to study nonlinear optical processes of probes in membranes.

The simulations provide abundant data and information for analysis: dynamical information, like that the membrane association process occurs within 10 ns; nature of interaction, like that the probe−membrane interaction has dominant contributions from van der Waals rather than from the electrostatic part, opposite to the case of the probe−water subsystem below 10 ns, conveying a picture that the probe−membrane interactions are mostly hydrophobic in nature while the probe−solvent interactions have large hydrophilic character; structural information, like that the integration of the probe into the membrane is associated with an exposure of the amide and peptide groups to the water solvent, while the aromatic and dimethylamino groups are buried into the membrane; spectroscopic information, like that the absorption spectra are attributed to a numerical red shift when going into the membrane; and design principles for improved probes, like that an increase of charge transfer character by substituting with electron-withdrawing and -donating groups in NAAA will yield improved two-photon imaging. Having demonstrated the principal qualities and the possibilities of the integrated quantum-mechanical/molecular mechanical approach for membrane probe simulations, we are now ready to take on specific applications in experimental collaboration.

■ ASSOCIATED CONTENT

Supporting Information

Representative snapshot configurations used in the property calculation for the cases where the probe is immersed in water and when it is associated to membrane, average density of solvated probe−membrane system as a function of *z*-axis, time evolution of center of mass components of the probe, radial distribution function of the probe−water system, time evolution of a number of solvent molecules in the first and second solvation shells of the probe, and HOMO and LUMO orbitals of probe. This material is available free of charge via the Internet at http://pubs.acs.org.

■ AUTHOR INFORMATION

Corresponding Author

agren@theochem.kth.se

Notes

The authors declare no competing financial interest.

■ ACKNOWLEDGMENTS

This work was supported by a grant from the Swedish Infrastructure Committee (SNIC) for the project ″Multiphysics Modeling of Molecular Materials″, SNIC 023/07-18. This work has been partially funded by the EU Commission (contract INFSO-RI-261523) through collaboration with ScalaLife (www.scalalife.eu). J.K. thanks the Danish Center for Scientific Computing (DCSC), The Danish Councils for Independent Research (The Sapere Aude programme), the Lundbeck Foundation, and the Villum foundation for financial support. H.Å. and E.L. thank Swedish e-Science Research Center (SeRC) for financial support.

■ REFERENCES

(1) McNeil, P. L.; Steinhardt, R. A. *Annu. Rev. Cell Dev. Biol.* **2003**, *19*, 697−731.
(2) Waggoner, A. S. *Ann. Rev. Biophys. Biol.* **1979**, *8*, 47−68.
(3) Matson, M.; Carlsson, N.; Beke-Somfai, T.; Nordén, B. *Langmuir* **2012**, *28*, 10808−10817.
(4) Reichardt, C. *Chem. Rev.* **1994**, *94*, 2319−2358.
(5) Alparone, A. *Phys. Chem. Chem. Phys.* **2013**, *15*, 12958−12962.
(6) Denk, W.; Strickler, J.; Webb, W. W. *Science* **1990**, *248*, 73−76.
(7) Zoumi, A.; Yeh, A.; Tromberg, B. J. *Proc. Natl. Acad. Sci. U.S.A.* **2002**, *99*, 11014−11019.
(8) Blanchard-Desce, M.; Ventelon, L.; Charier, S.; Moreaux, L.; Mertz, J. *Proc. SPIE* **2001**, *4461*, 20.
(9) Schulz, R.; Lindner, B.; Petridis, L.; Smith, J. C. *J. Chem. Theory Comput.* **2009**, *5*, 2798−2808.
(10) Fantacci, S.; Angelis, F. D.; Sgamellotti, A.; Marrone, A.; Re, N. *J. Am. Chem. Soc.* **2005**, *127*, 14144−14145.
(11) Murugan, N. A.; Kongsted, J.; Rinkevicius, Z.; Ågren, H. *Phys. Chem. Chem. Phys.* **2012**, *14*, 1107−1112.
(12) Murugan, N. A.; Olsen, J. M. H.; Kongsted, J.; Rinkevicius, Z.; Aidas, K.; Ågren, H. *J. Phys. Chem. Lett.* **2013**, *4*, 70−77.
(13) Mereau, R.; Castet, F.; Botek, E.; Champagne, B. *J. Phys. Chem. A* **2009**, *113*, 6552−6554.
(14) Wong, J.; Duchscherer, T.; Pietraru, G.; Cramb, D. *Langmuir* **1999**, *15*, 6181−6186.
(15) Moyano, F.; Biasutti, M. A.; Silber, J. J.; Correa, N. M. *J. Phys. Chem. B* **2006**, *110*, 11838−11846.
(16) Chong, P. L. G. *Biochemistry* **1988**, *27*, 399−404.
(17) Mennucci, B.; Caricato, M.; Ingrosso, F.; Cappelli, C.; Cammi, R.; Tomasi, J.; Scalmani, G.; Frisch, M. J. *J. Phys. Chem. B* **2008**, *112*, 414−423.
(18) Nitschke, W. K.; Vequi-Suplicy, C. C.; Coutinho, K.; Stassen, H. *J. Phys. Chem. B* **2012**, *116*, 2713−2721.
(19) Cwiklik, L.; Aquino, A. J. A.; Vazdar, M.; Jurkiewicz, P.; Pittner, J.; Hof, M.; Lischka, H. *J. Phys. Chem. A* **2011**, *115*, 11428−11437.
(20) Yu, W.; So, P. T. C.; French, T.; Gratton, E. *Biophys. J.* **1996**, *70*, 626−636.
(21) Kim, H. M.; Choo, H.-J.; Jung, S.-Y.; Ko, Y.-G.; Park, W.-H.; Jeon, S.-J.; Kim, C. H.; Joo, T.; Cho, B. R. *ChemBioChem.* **2007**, *8*, 553−559.
(22) Cohen, B.; McAnaney, T.; Park, E.; Jan, Y.; Boxer, S.; Jan, L. *Science* **2002**, *296*, 1700−1703.
(23) Abbyad, P.; Shi, X.; Childs, W.; McAnaney, T. B.; Cohen, B. E.; Boxer, S. G. *J. Phys. Chem. B* **2007**, *111*, 8269−8276.
(24) Zipfel, W. R.; Williams, R. M.; Webb, W. W. *Nat. Biotechnol.* **2003**, *21*, 1369−1377.

(25) Kucherak, O. A.; Didier, P.; Mély, Y.; Klymchenko, A. S. *J. Phys. Chem. Lett.* **2010**, *1*, 616−620.
(26) Gaus, K.; Zech, T.; Harder, T. *Mol. Membr. Biol.* **2006**, *23*, 41−48.
(27) wan Myung, Kim; Kim, B. R.; Choo, H.-J.; Ko, Y.-G.; Jeon, S.-J.; Kim, C. H.; Joo, T.; Cho, B. R. *ChemBioChem.* **2008**, *9*, 2830−2838.
(28) Wang, J.; Wolf, R.; Caldwell, J.; Kollman, P.; Case, D. *J. Comput. Chem.* **2004**, *34*, 1157−1174.
(29) Breneman, C.; Wiberg, K. *J. Comput. Chem.* **1990**, *11*, 361−373.
(30) Frisch, M. J. et al. *Gaussian 09*, Revision A.02; Gaussian, Inc.: Wallingford, CT, 2009.
(31) Berger, O.; Edholm, O.; Jähnig, F. *Biophys. J.* **1997**, *72*, 2002−2013.
(32) Berendsen, H. J. C.; Grigera, J. R.; Straatsma, T. P. *J. Phys. Chem.* **1987**, *91*, 6269−6271.
(33) Bussi, G.; Donadio, D.; Parrinello, M. *J. Chem. Phys.* **2007**, *126*, 014101.
(34) Parrinello, M.; Rahman, A. *Phys. Rev. Lett.* **1980**, *45*, 1196−1199.
(35) Pronk, S.; Páll, S.; Schulz, R.; Larsson, P.; Bjelkmar, P.; Apostolov, R.; Shirts, M.; Smith, J.; Kasson, P.; van der Spoel, D.; Hess, B.; Lindahl, E. *Bioinformatics* **2013**, *7*, 845−54.
(36) Olsen, J. M.; Aidas, K.; Kongsted, J. *J. Chem. Theory Comput.* **2010**, *6*, 3721−3734.
(37) Perry, S. W.; Bruke, R. M.; Brown, E. B. *Protein Sci.* **1993**, *2*, 404−410.
(38) Li, X.; Rinkevicius, Z.; Kongsted, J.; Murugan, N. A.; Ågren, H. *J. Chem. Theory Comput.* **2012**, *8*, 4766−4774.
(39) Albota, M.; et al. *Science* **1998**, *281*, 1653−1656.
(40) Day, P. N.; Nguyen, K. A.; Pachter, R. *J. Phys. Chem. B* **2005**, *109*, 1803−1814.
(41) Chakrabarti, S.; Ruud, K. *Phys. Chem. Chem. Phys.* **2009**, *11*, 2592−2596.
(42) Murugan, N. A.; Kongsted, J.; Rinkevicius, Z.; Aidas, K.; Mikkelsen, K. V.; Ågren, H. *Phys. Chem. Chem. Phys.* **2011**, *13*, 12506−12516.
(43) Peach, M. J. G.; Benfield, P.; Helgaker, T.; Tozer, D. J. *J. Chem. Phys.* **2008**, *128*, 044118.
(44) Moreaux, L.; Sandre, O.; Blanchard-Desce, M.; Mertz, J. *Opt. Lett.* **2000**, *25*, 320−322.
(45) Perry, S. W.; Bruke, R. M.; Brown, E. B. *Ann. Biomed. Eng.* **2012**, *40*, 277−291.
(46) Kanis, D.; Ratner, M.; Marks, T. *Chem. Rev.* **1994**, *94*, 195−242.
(47) Murugan, N. A.; Kongsted, J.; Rinkevicius, Z.; Ågren, H. *Proc. Natl. Acad. Sci. U.S.A.* **2010**, *107*, 16453−16458.